SUPPORTING INFORMATION

Patient-Specific Nanoparticle Targeting in Human Leukemia Blood

Yi Ju,[1,2] Shiyao Li,[1] Abigail Er Qi Tan,[2] Emily H. Pilkington,[2] Paul T. Brannon,[3] Magdalena Plebanski,[4] Jiwei Cui,[5] Frank Caruso,[6] Kristofer J. Thurecht,[7] Constantine Tam,[8,9] and Stephen J. Kent[2,10]**

[1]School of Science, RMIT University, Melbourne, Victoria 3000, Australia

[2]Department of Microbiology and Immunology, Peter Doherty Institute for Infection and Immunity, The University of Melbourne, Melbourne, Victoria 3000, Australia

[3]Materials Characterisation and Fabrication Platform, The University of Melbourne, Parkville, Victoria 3010, Australia

[4]School of Health and Biomedical Sciences, RMIT University, Bundoora, Victoria 3083, Australia

[5]Key Laboratory of Colloid and Interface Chemistry of the Ministry of Education, School of Chemistry and Chemical Engineering, Shandong University, Jinan, Shandong 250100, China

[6]Department of Chemical Engineering, The University of Melbourne, Parkville, Victoria 3010, Australia

[7]Australian Institute for Bioengineering and Nanotechnology, University of Queensland, St Lucia 4072, Australia

[8]Department of Clinical Haematology, The Royal Melbourne Hospital and Peter MacCallum Cancer Centre, Melbourne, Victoria 3000, Australia

[9]Faculty of Medicine, Dentistry and Health Sciences, The University of Melbourne, Melbourne, Victoria, 3000, Australia

[10]Melbourne Sexual Health Centre and Department of Infectious Diseases, Alfred Hospital and Central Clinical School, Monash University, Melbourne, Victoria 3000, Australia

*Corresponding authors. E-mail: david.ju@rmit.edu.au; skent@unimelb.edu.au.

Table S1. Average size and zeta potential of PEG, PEG-MS, and Doxil nanoparticles before and after functionalized with BsAbs

Particle	Size (nm)[a]	Polydispersity Index[a]	Zeta Potential (mV)[b]
PEG	632 ± 91	–	−1 ± 6
PEG-CD20	650 ± 94	–	−1 ± 3
PEG-CD28	664 ± 75	–	−1 ± 4
PEG-MS	467 ± 119	0.017	−31 ± 5
PEG-MS-CD20	459 ± 119	0.010	−27 ± 5
PEG-MS-CD28	453 ± 111	0.031	−29 ± 4
Doxil	75 ± 19	0.048	−13 ± 9
Doxil-CD20	84 ± 26	0.085	−9 ± 6
Doxil-CD28	81 ± 27	0.13	−10 ± 6

[a]The size and polydispersity index of the PEG-MS and Doxil nanoparticles with and without BsAB (CD20 or C28) functionalization were determined by DLS. The size of the PEG particles with and without BsAb (CD20 or CD28) functionalization was determined from SIM images. [b]Zeta potential measurements were performed at pH 7.2 in phosphate buffer (5 mM).

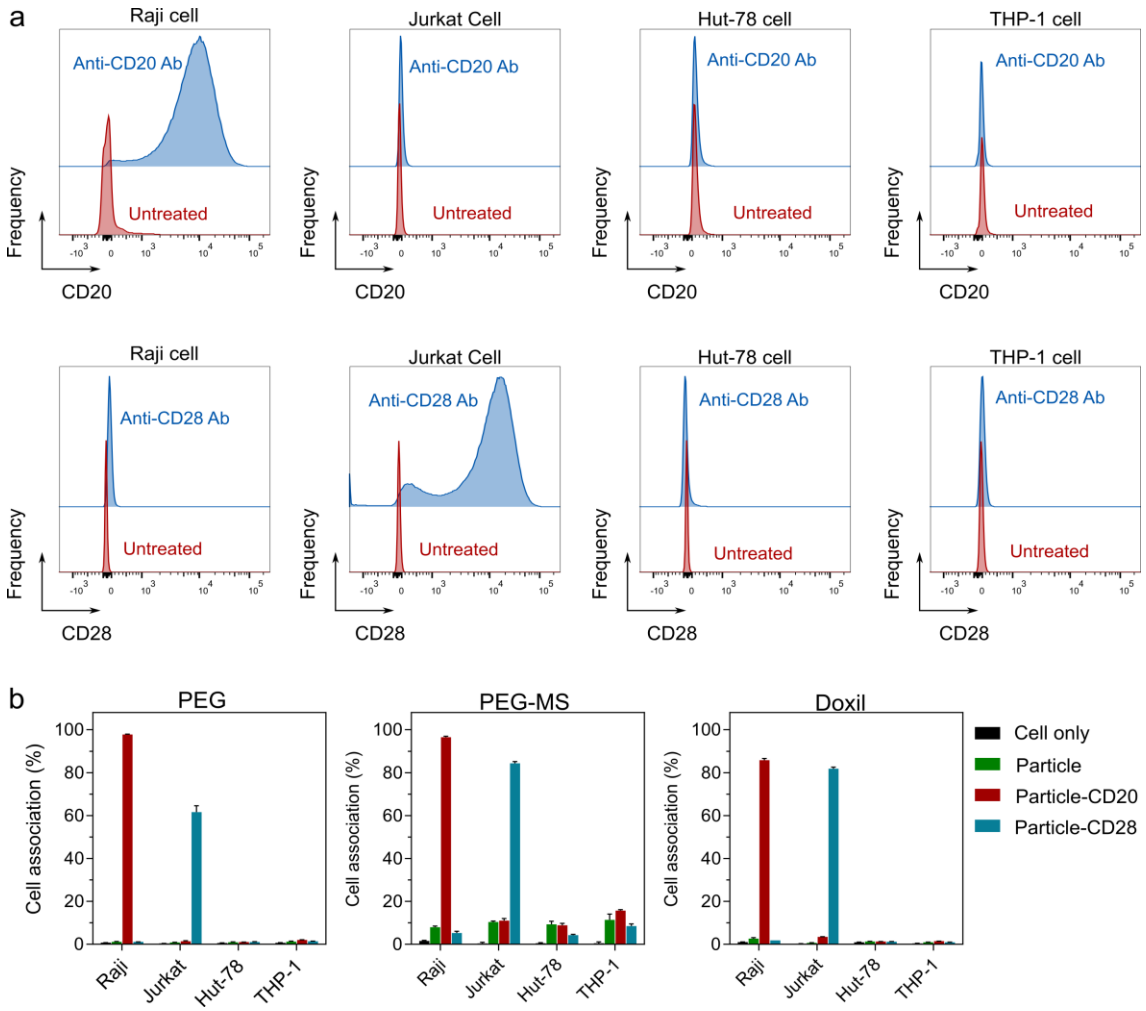

Figure S1. Evaluation of cancer cell targeting using conventional cell line models. (a) CD20 and CD28 expression of Raji, Jurkat, Hut-78, and THP-1 cell lines. Cells were treated with fluorescence-labeled anti-human CD20 or CD28 antibodies (Ab) and then analyzed by flow cytometry. (b) Cell targeting of nonfunctionalized and BsAb-functionalized PEG, PEG-MS, and Doxil nanoparticles using four cell lines: Raji, Jurkat, Hut-78, and THP-1. Particles were incubated with cells for 1 h at 37 °C and then analyzed by flow cytometry. Cell association (%) refers to the proportion of each cell type with positive fluorescence, above background, stemming from fluorescence-labeled particles. Cell association (%) data are shown as the mean ± standard deviation (SD) of three independent experiments (using fresh blood from the same donor), with at least 40,000 cells analyzed for each experimental condition studied. Cell only control groups represent the respective cell populations without particle incubation.

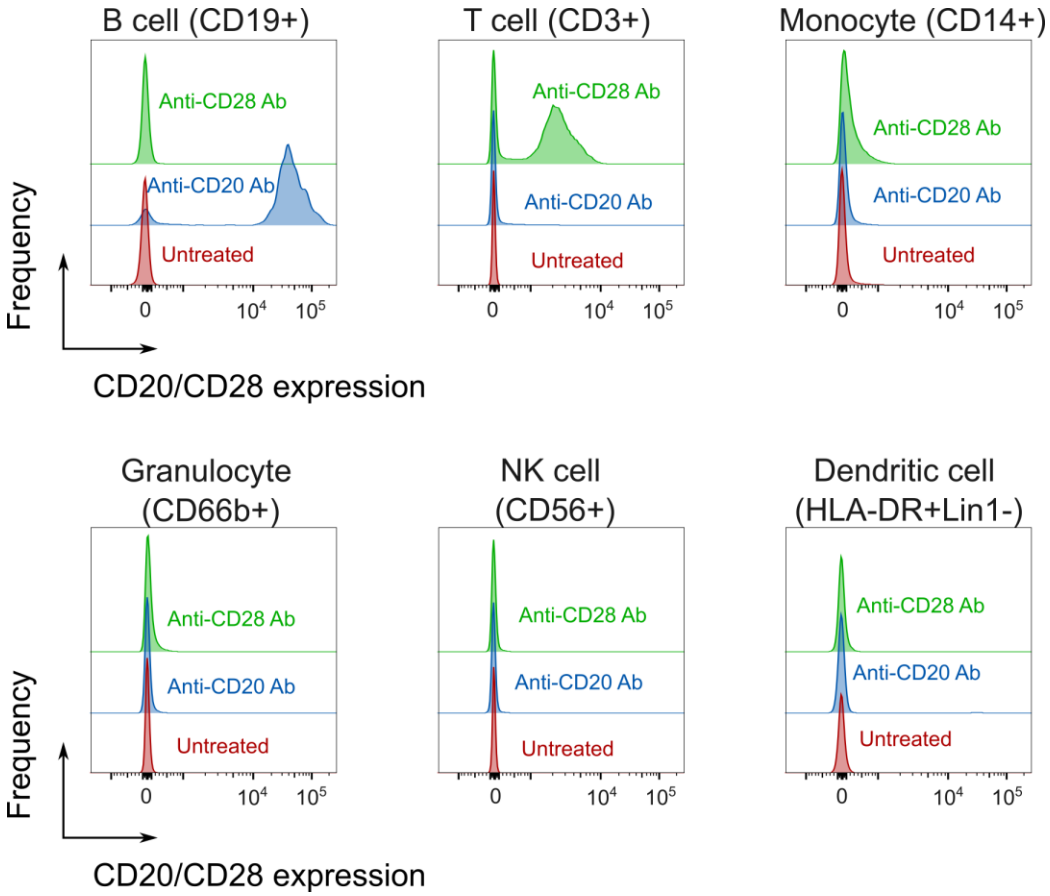

Figure S2. CD20 and CD28 expression in blood immune cells from a healthy donor. Fresh human blood was treated with fluorescence-labeled anti-human CD20 or CD28 Ab, and cells were phenotyped with antibody cocktails and analyzed by flow cytometry.

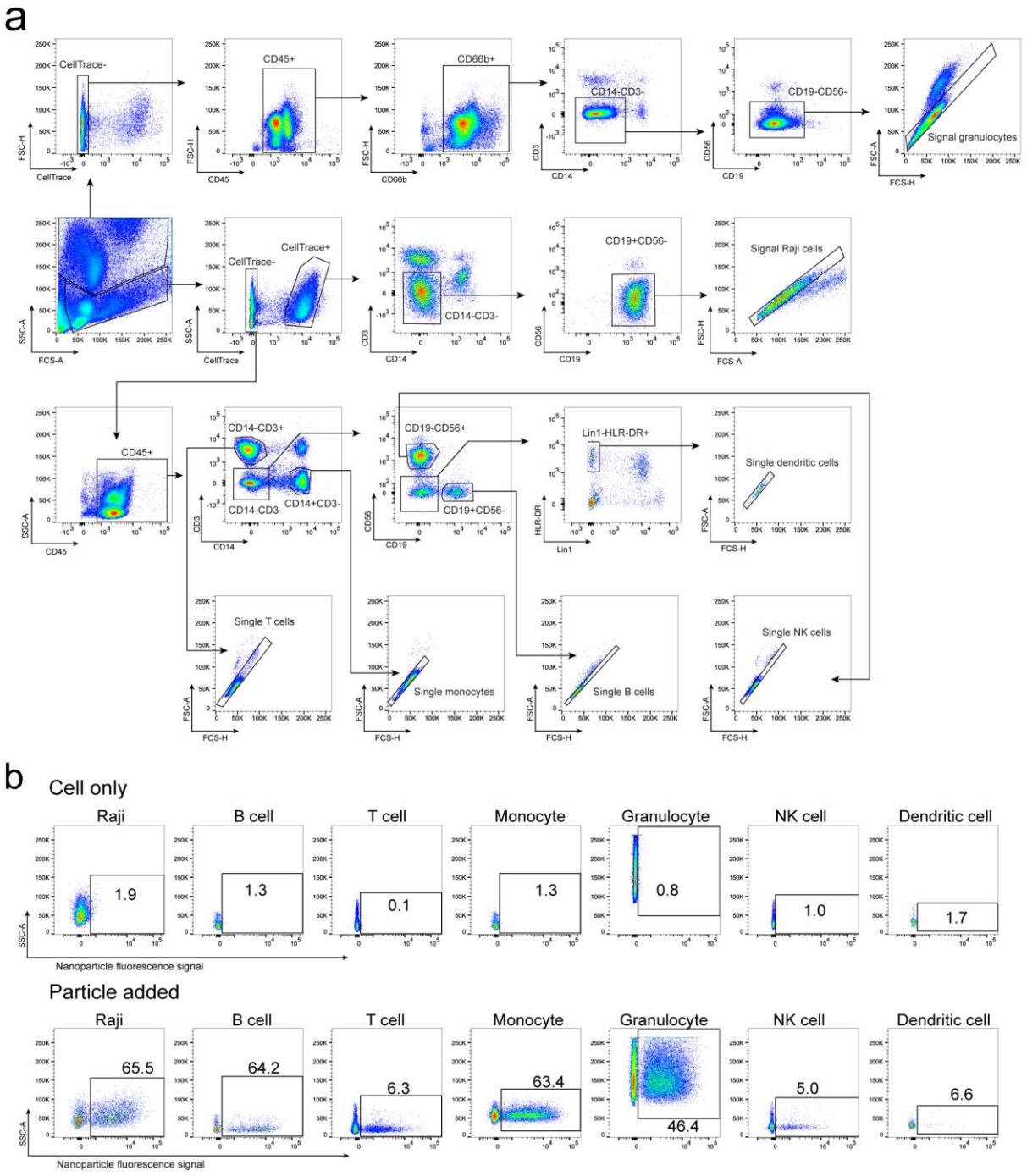

Figure S3. Gating strategy used to identify Raji cells and white blood cell population of the whole human blood model, wherein Raji cells are spiked into fresh whole blood of a healthy donor. (a) Flow cytometry gating strategy used to identify Raji cells and different immune cell populations from human blood. Raji cells were prelabeled with CellTrace yellow cell proliferation kit and then added into fresh human blood from a healthy donor, followed by incubation with nanoparticles for 1 h at 37 °C and subsequent analysis by flow cytometry. (b)

The percentage of each cell type positive for the fluorescence-labeled nanoparticles was then measured as the cell association (%). The representative gating strategy and cell association percentages for each cell type are shown.

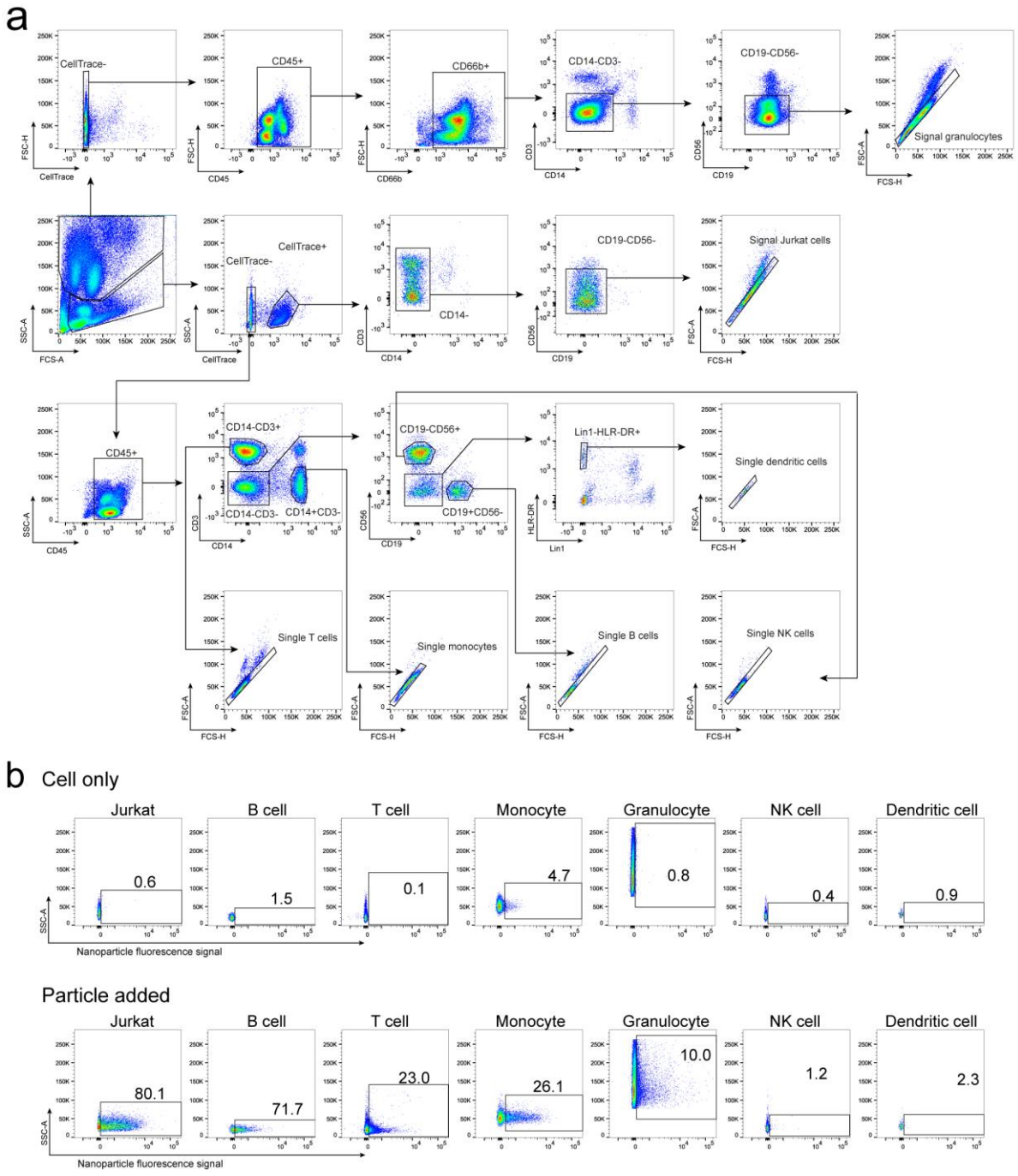

Figure S4. Gating strategy used to identify Jurkat cells and white blood cell population of the whole human blood model, wherein Jurkat cells are spiked into fresh whole blood of a healthy donor. (a) Flow cytometry gating strategy used to identify Jurkat cells and different immune cell populations from human blood. Jurkat cells were prelabeled with CellTrace yellow cell proliferation kit and then added into fresh human blood from a healthy donor, followed by incubation with nanoparticles for 1 h at 37 ℃ and subsequent analysis by flow cytometry. (b)

The percentage of each cell type positive for the fluorescence-labeled nanoparticles was then measured as the cell association (%). The representative gating strategy and cell association percentages for each cell type are shown.

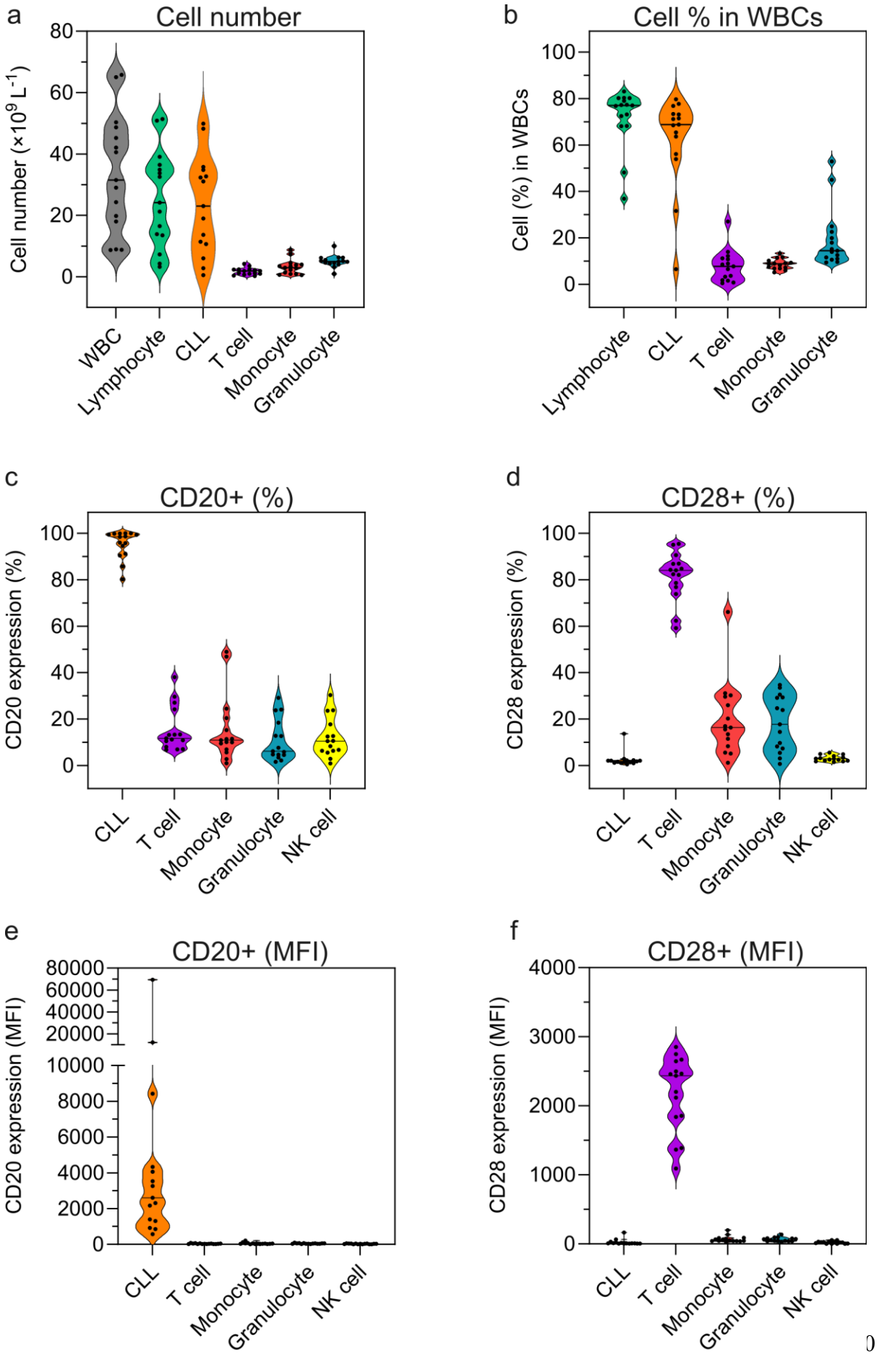
a
Cell number
Cell number (×10^9 L^-1)
WBC
Lymphocyte
CLL
T cell
Monocyte
Granulocyte
b
Cell % in WBCs
Cell (%) in WBCs
Lymphocyte
CLL
T cell
Monocyte
Granulocyte
c
CD20+ (%)
CD20 expression (%)
CLL
T cell
Monocyte
Granulocyte
NK cell
d
CD28+ (%)
CD28 expression (%)
CLL
T cell
Monocyte
Granulocyte
NK cell
e
CD20+ (MFI)
CD20 expression (MFI)
CLL
T cell
Monocyte
Granulocyte
NK cell
f
CD28+ (MFI)
CD28 expression (MFI)
CLL
T cell
Monocyte
Granulocyte
NK cell

Figure S5. Cell count and expression of CD20 and CD28 in blood immune cells from CLL patients (n = 15). (a,b) Cell count and cell percentage in white blood cells were obtained from a CELL-DYN Emerald analyzer. CLL cell count was obtained from flow cytometry. (c-e) CD20 and CD28 expression of white blood cells from CLL patients. Fresh CLL blood was treated with fluorescence-labeled anti-human CD20 or CD28 antibodies, followed by phenotyping cells with antibody cocktails and analysis by flow cytometry. CD20 and CD28 expressions are presented as (c,d) the percentage of cells expressing CD20 or CD28, and (e,f) the median fluorescence index (MFI) of each cell type, stemming from fluorescence-labeled anti-human CD20 or CD28 antibodies. WBC, white blood cell.

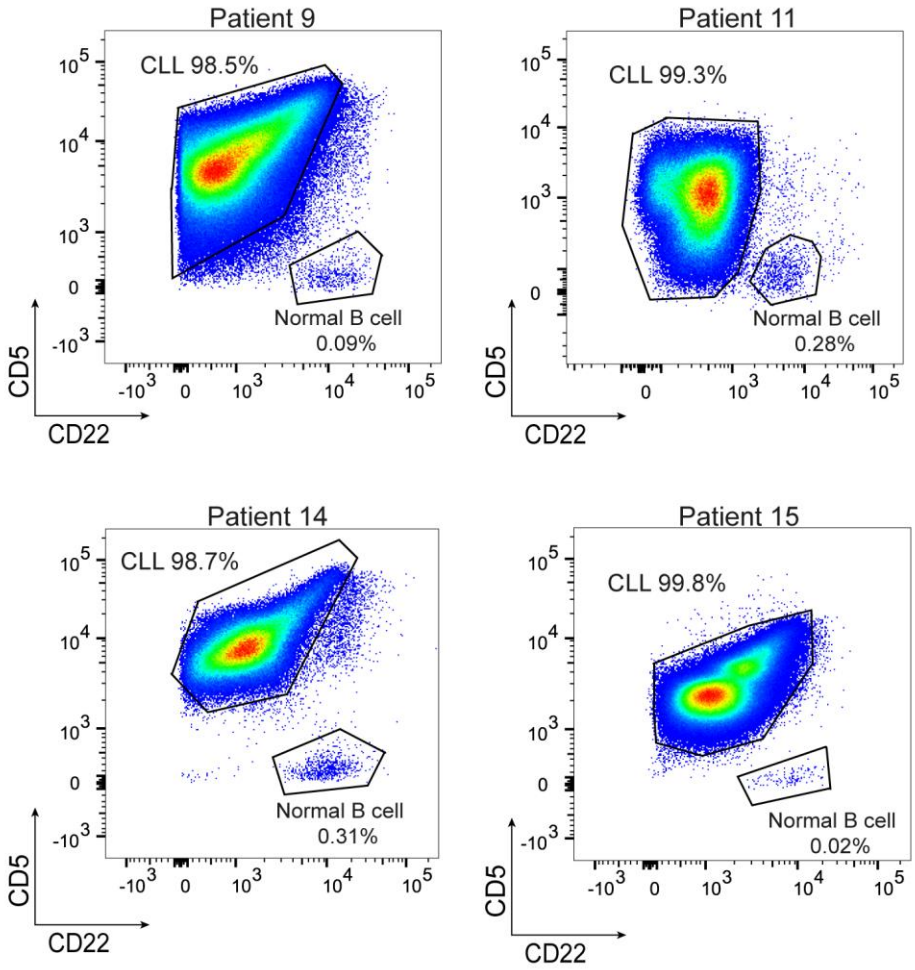

Figure S6. Gating strategy used to distinguish between CLL and normal B cells. Out of the 15 CLL patients, only 4 patients have normal B cells identified in the blood with less than 0.5% of total CD19+ B cells. The gating strategy was established based on a previous report on the immunophenotypic profiles of CLL and normal B cells.[1]

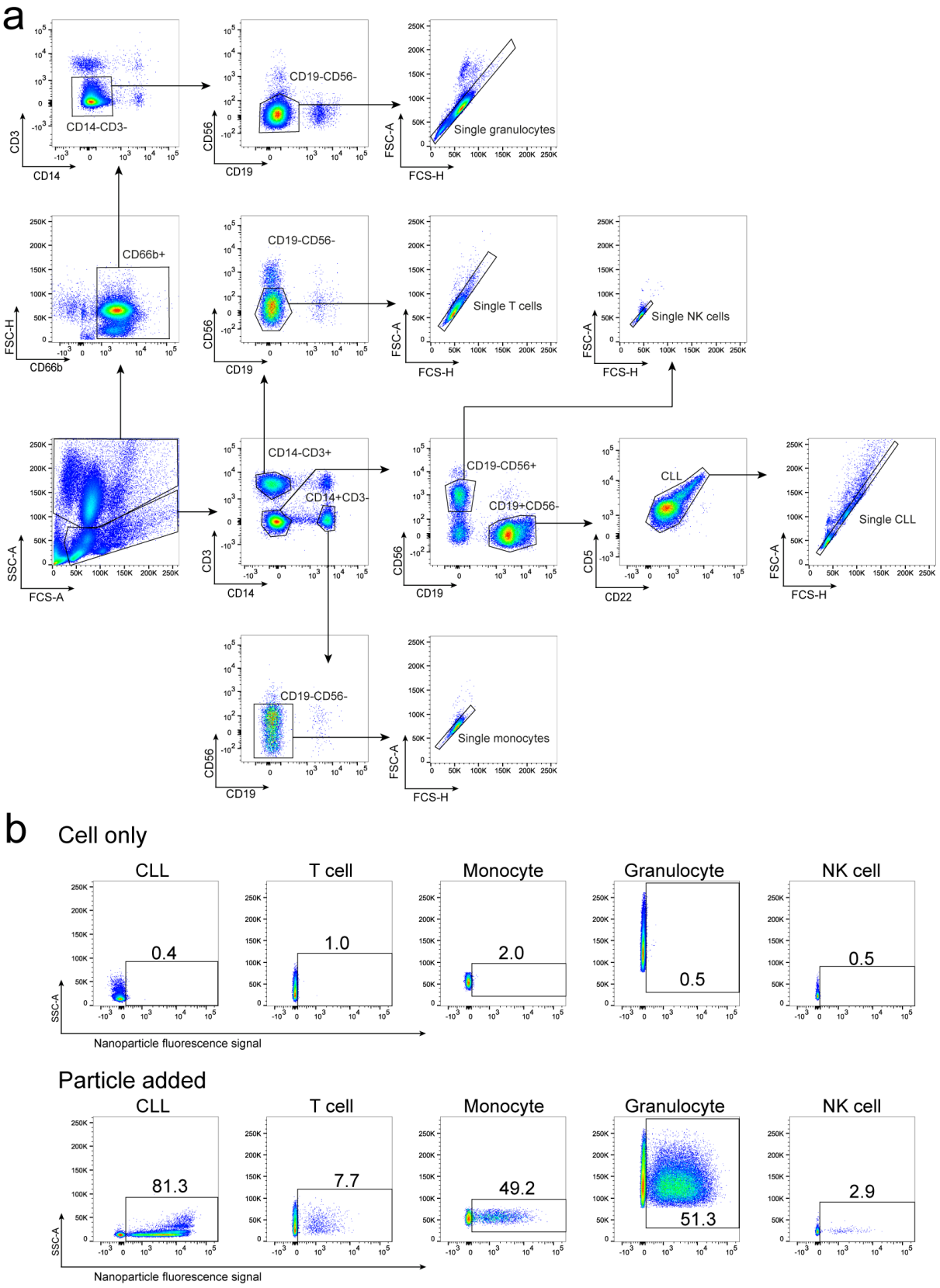

Figure S7. Gating strategy used to identify CLL cells and white blood cell population of the whole blood from CLL patients. (a) Flow cytometry gating strategy used to identify CLL cells

and different immune cell populations from blood of CLL patients. (b) The percentage of each cell type positive for the fluorescence-labeled nanoparticles was then measured as the cell association (%). The representative gating strategy and cell association percentages for each cell type are shown.

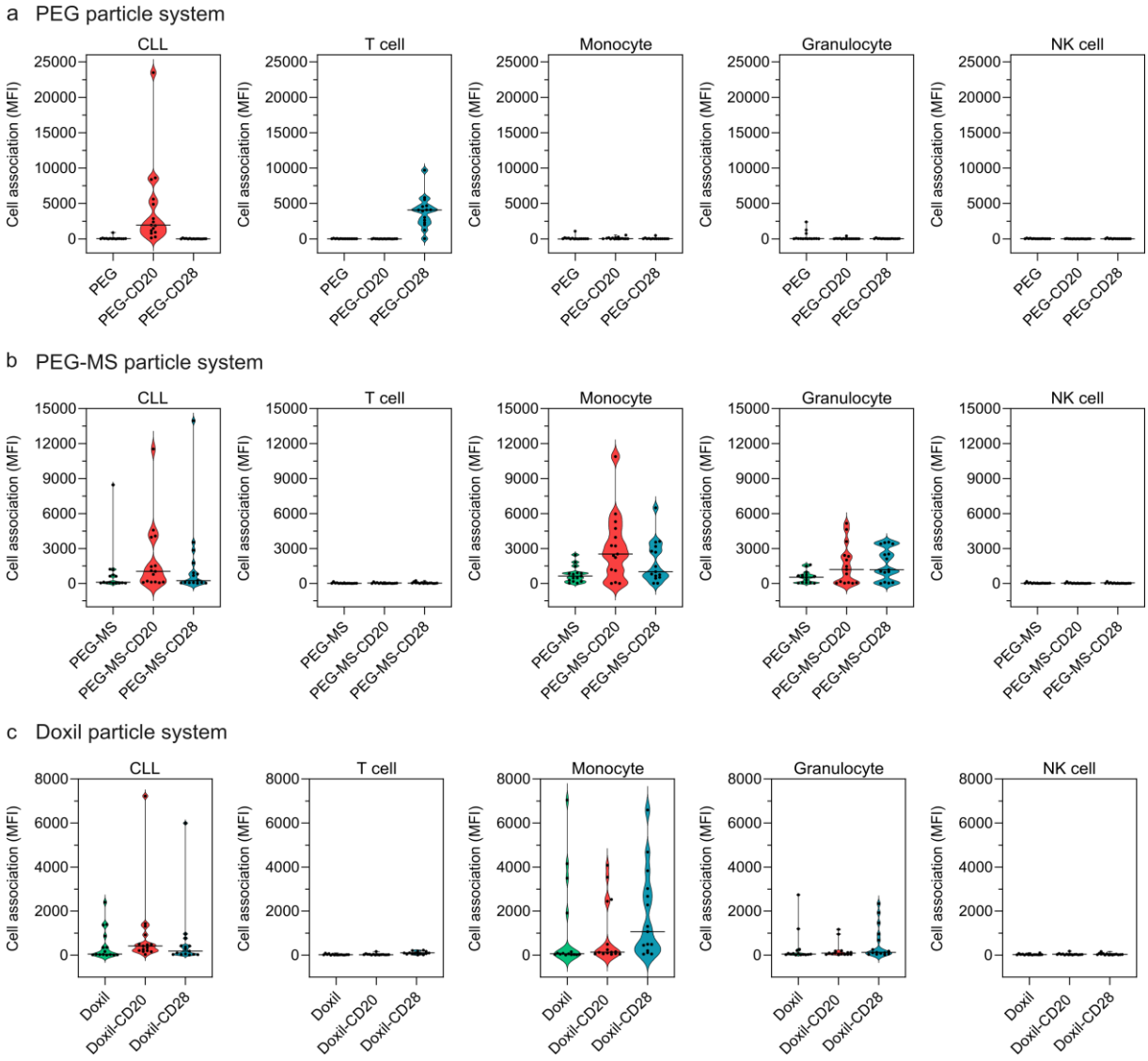

Figure S8. (a–c) Violin plots summarizing cell association (MFI) of the nonfunctionalized and BsAb-functionalized PEG (a), PEG-MS (b), and Doxil (c) nanoparticles in the blood of 15 CLL patients after 1 h incubation at 37 °C. Cell association (MFI) refers to the median fluorescence index of each cell type, stemming from fluorescence-labeled particles. Each data point is the mean of three independent experiments (using the same batch of fresh blood from each donor). The median cell association (MFI) across 15 CLL patients is shown as a solid line in the violin plots.

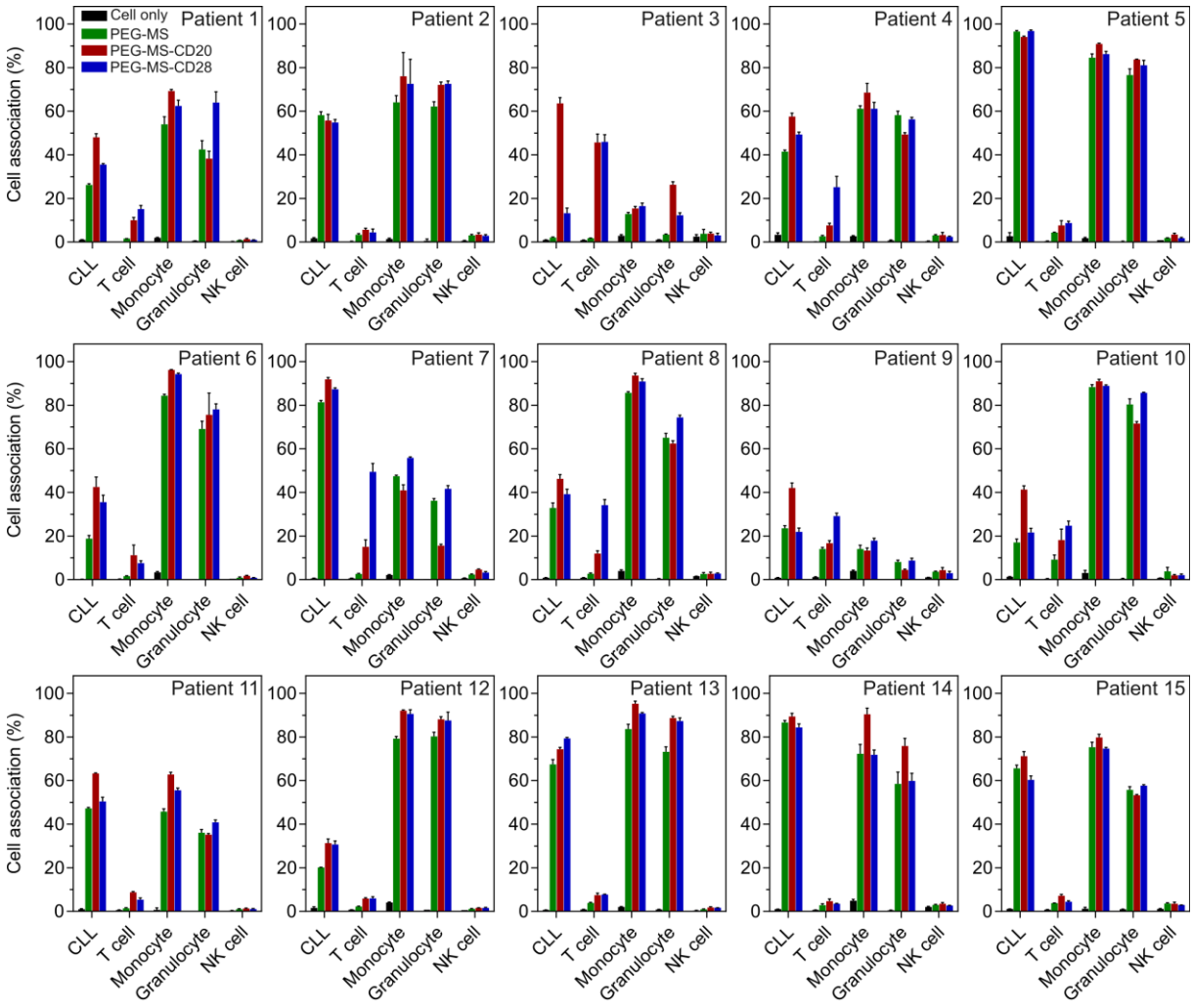

Figure S9. CLL targeting of nonfunctionalized and BsAb-functionalized PEG-MS particles in the whole blood of the 15 CLL patients. Cell association (%) refers to the proportion of each cell type with positive fluorescence, above background, stemming from fluorescence-labeled particles (see gating strategy in Figure S7). Cell association (%) data are shown as the mean ± SD of three independent experiments (using fresh blood from each donor), with at least 400,000 leukocytes analyzed for each experimental condition studied. Cell only control groups represent the respective cell populations without particle incubation.

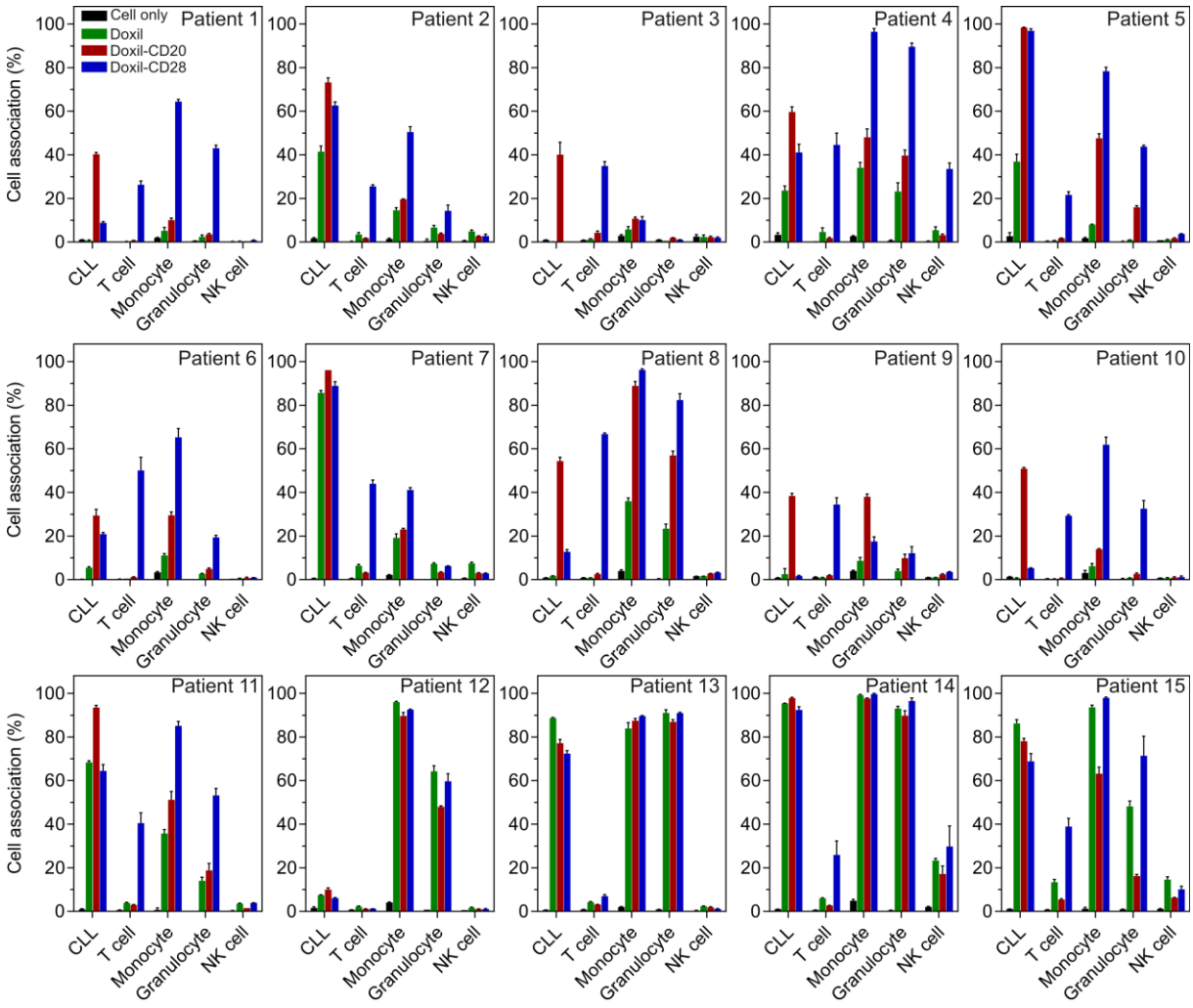

Figure S10. CLL targeting of nonfunctionalized and BsAb-functionalized Doxil nanoparticles in the whole blood of the 15 CLL patients. Cell association (%) refers to the proportion of each cell type with positive fluorescence, above background, stemming from fluorescence-labeled particles (see gating strategy in Figure S7). Cell association (%) data are shown as the mean ± SD of three independent experiments (using fresh blood from each donor), with at least 400,000 leukocytes analyzed for each experimental condition studied. Cell only control groups represent the respective cell populations without particle incubation.

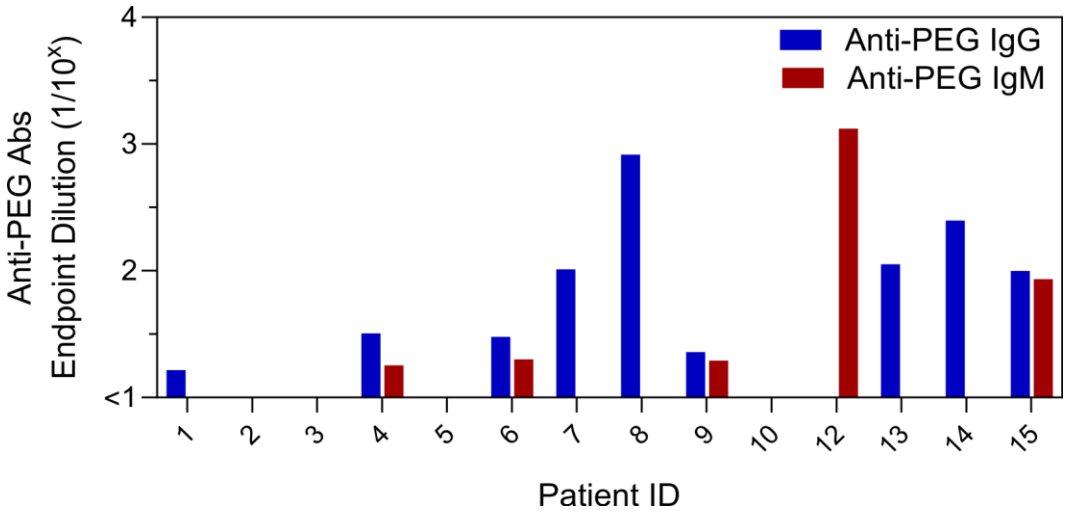

Figure S11. Plasma anti-PEG IgG and IgM titers of 14 CLL patients. Data are shown as the mean of two independent measurements (recruitment of Patient 11 was delayed and occurred after this experiment was performed and thus not included in the assay).

a Anti-PEG IgG versus PEG−monocyte association

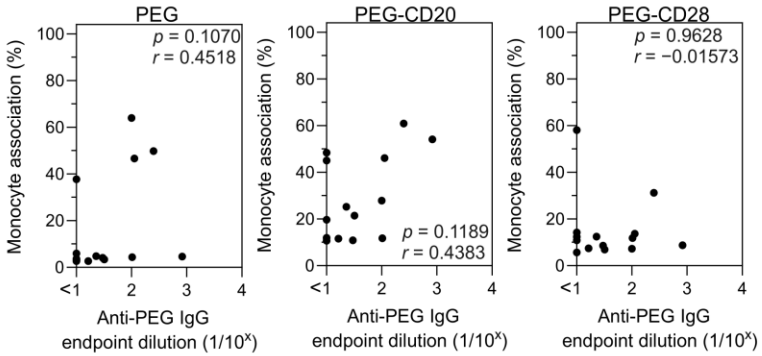

b Anti-PEG IgG versus PEG-MS−monocyte association

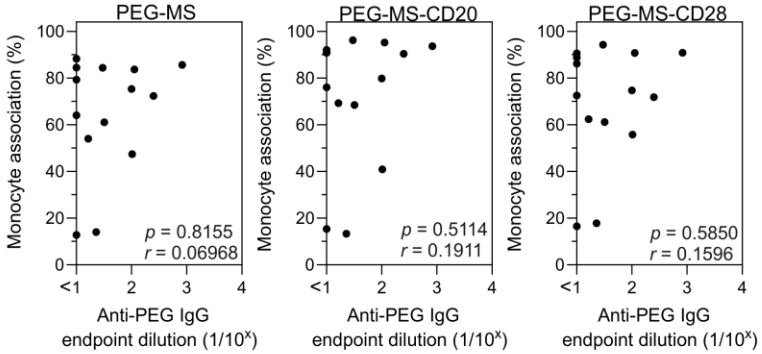

c Anti-PEG IgG versus Doxil−monocyte association

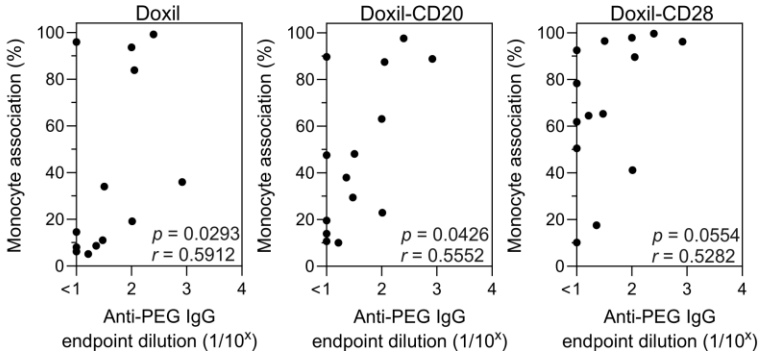

d Anti-PEG IgG versus PEG−granulocyte association

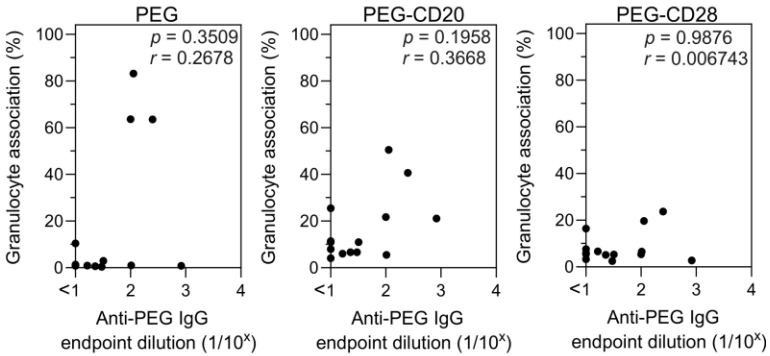

e Anti-PEG IgG versus PEG-MS−granulocyte association

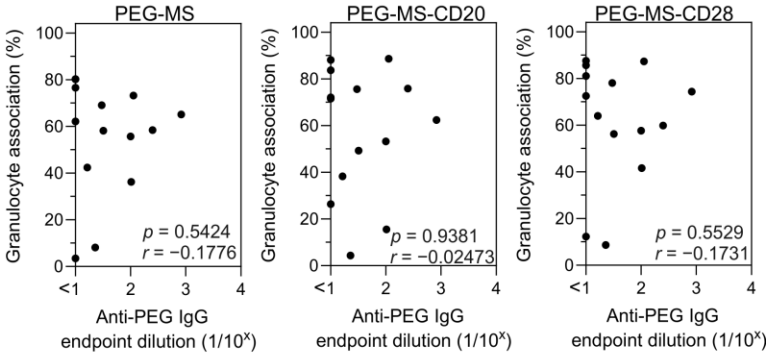

f Anti-PEG IgG versus Doxil−granulocyte association

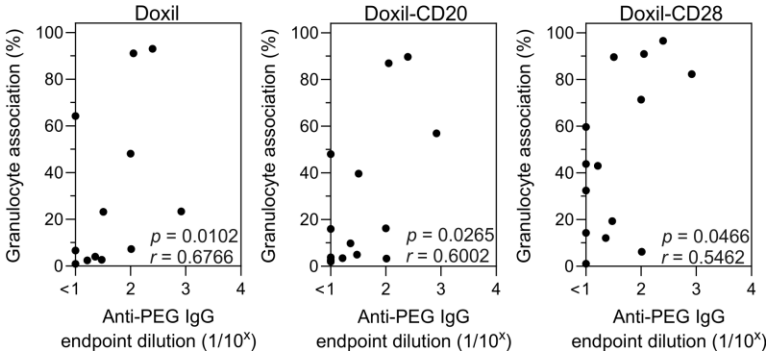

Figure S12. Spearman correlation analysis between plasma anti-PEG IgG titers and (a–c) monocyte or (d–f) granulocyte association (%) with PEG, PEG-MS, and Doxil nanoparticles with and without functionalization of anti-PEG/anti-CD20 or anti-PEG/anti-CD28 BsAb (n = 14).

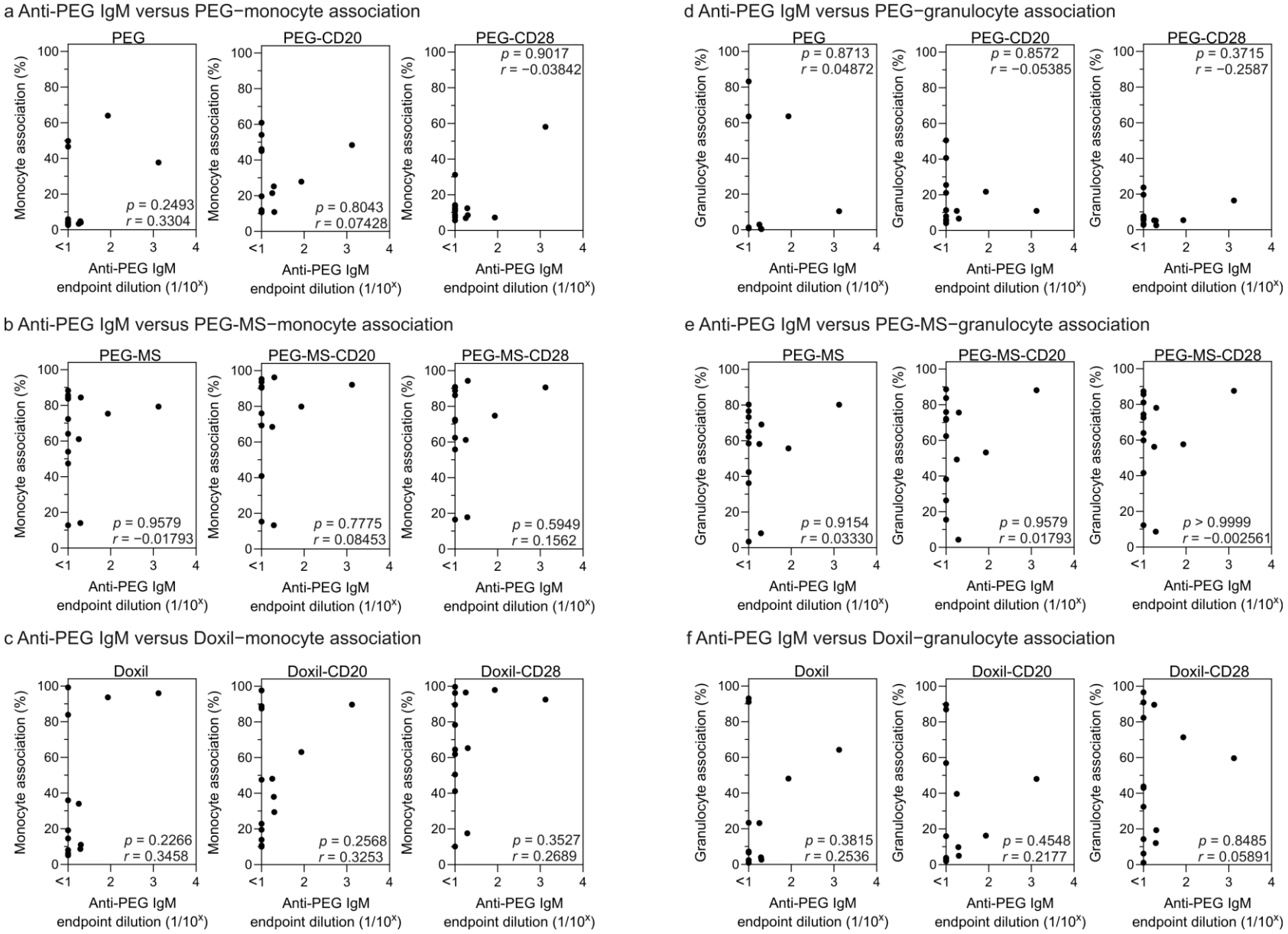
a Anti-PEG IgM versus PEG−monocyte association
PEG
PEG-CD20
PEG-CD28
p = 0.2493
r = 0.3304
p = 0.8043
r = 0.07428
p = 0.9017
r = −0.03842
b Anti-PEG IgM versus PEG-MS−monocyte association
PEG-MS
PEG-MS-CD20
PEG-MS-CD28
p = 0.9579
r = −0.01793
p = 0.7775
r = 0.08453
p = 0.5949
r = 0.1562
c Anti-PEG IgM versus Doxil−monocyte association
Doxil
Doxil-CD20
Doxil-CD28
p = 0.2266
r = 0.3458
p = 0.2568
r = 0.3253
p = 0.3527
r = 0.2689
d Anti-PEG IgM versus PEG−granulocyte association
PEG
PEG-CD20
PEG-CD28
p = 0.8713
r = 0.04872
p = 0.8572
r = −0.05385
p = 0.3715
r = −0.2587
e Anti-PEG IgM versus PEG-MS−granulocyte association
PEG-MS
PEG-MS-CD20
PEG-MS-CD28
p = 0.9154
r = 0.03330
p = 0.9579
r = 0.01793
p > 0.9999
r = −0.002561
f Anti-PEG IgM versus Doxil−granulocyte association
Doxil
Doxil-CD20
Doxil-CD28
p = 0.3815
r = 0.2536
p = 0.4548
r = 0.2177
p = 0.8485
r = 0.05891
Monocyte association (%)
Granulocyte association (%)
Anti-PEG IgM
endpoint dilution (1/10x)
<1
0
20
40
60
80
100
1
2
3
4

Figure S13. Spearman correlation analysis between plasma anti-PEG IgM titers and (a–c) monocyte or (d–f) granulocyte association (%) with PEG, PEG-MS, or Doxil nanoparticles with and without functionalization of anti-PEG/anti-CD20 or anti-PEG/anti-CD28 BsAb (n = 14).

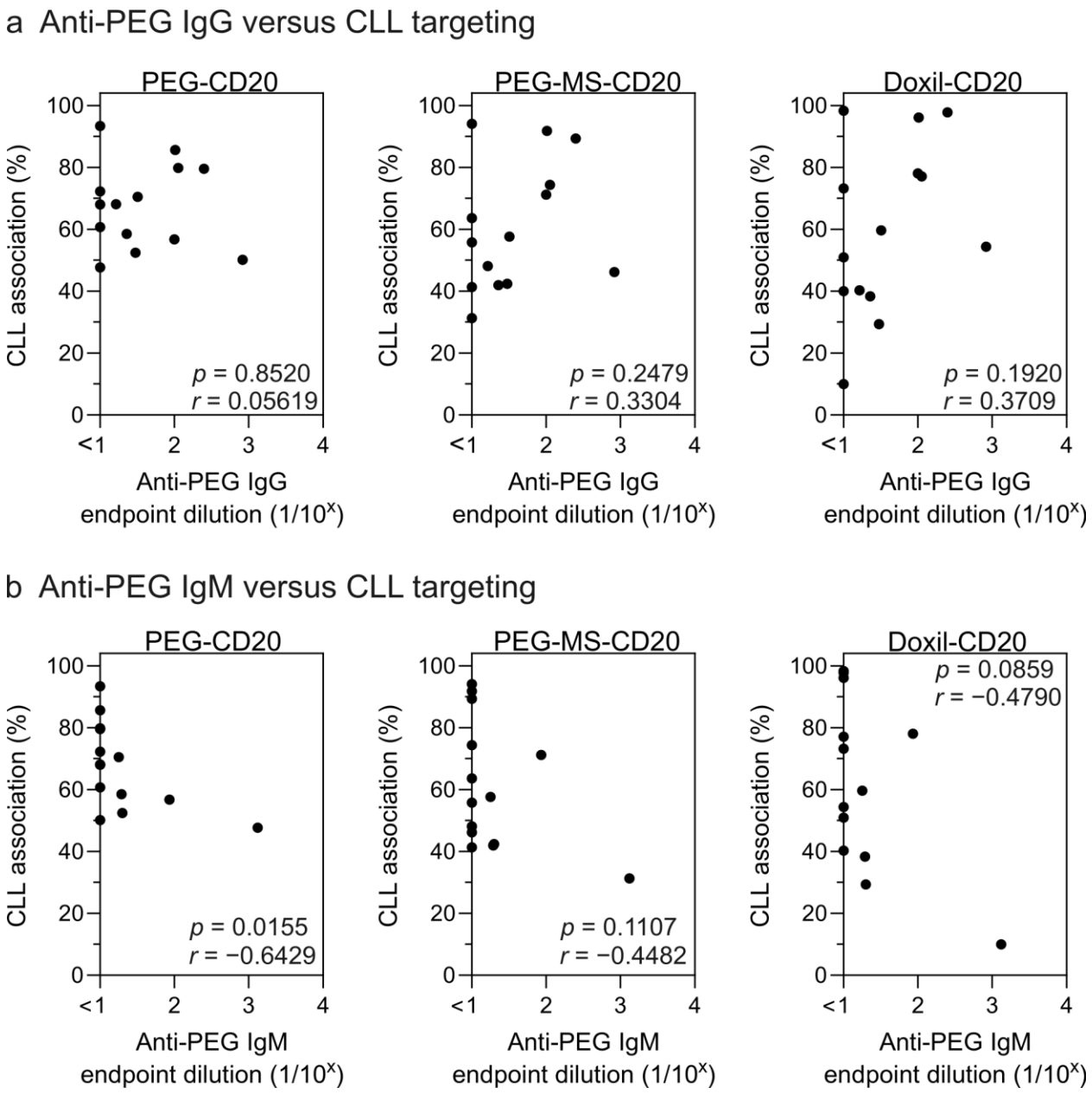

Figure S14. Spearman correlation analysis between plasma anti-PEG IgG or IgM titers and CLL targeting of PEG, PEG-MS, or Doxil nanoparticles functionalized with anti-PEG/anti-CD20 BsAbs (n = 14).

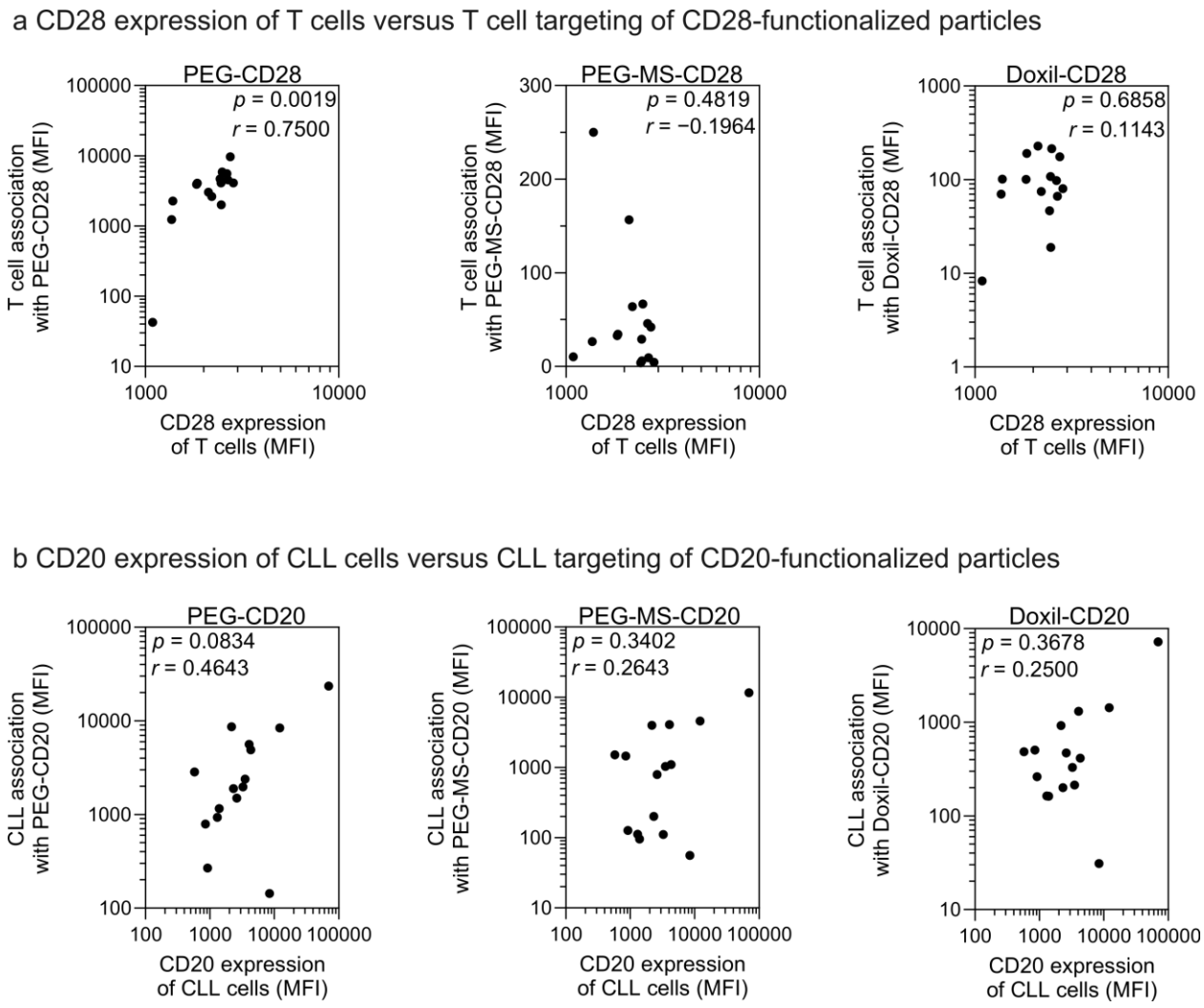

Figure S15. Spearman correlation analysis (a) between CD28 expression of T cells and T cell targeting by PEG, PEG-MS, or Doxil nanoparticles functionalized with anti-PEG/anti-CD28 BsAbs (n = 15), and (b) between CD20 expression of CLL cells and CLL cell targeting by PEG, PEG-MS, or Doxil nanoparticles functionalized with anti-PEG/anti-CD20 BsAbs (n = 15).

REFERENCES

(1) Rawstron, A. C.; Villamor, N.; Ritgen, M.; Böttcher, S.; Ghia, P.; Zehnder, J. L.; Lozanski, G.; Colomer, D.; Moreno, C.; Geuna, M.; Evans, P. A. S.; Natkunam, Y.; Coutre, S. E.; Avery, E. D.; Rassenti, L. Z.; Kipps, T. J.; Caligaris-Cappio, F.; Kneba, M.; Byrd, J. C.; Hallek, M. J.; Montserrat, E.; Hillmen, P. International Standardized Approach for Flow Cytometric Residual Disease Monitoring in Chronic Lymphocytic Leukaemia. *Leukemia* **2007**, *21*, 956.